Environ Sci Pollut Res (2018) 25:3731–3744
https://doi.org/10.1007/s11356-017-0663-1

RESEARCH ARTICLE

Visible light-induced photocatalytic degradation of Reactive Blue-19 over highly efficient polyaniline-TiO_2 nanocomposite: a comparative study with solar and UV photocatalysis

Shankramma Kalikeri[1] · **Nidhi Kamath**[2] · **Dhanashri Jayant Gadgil**[1] · **Vidya Shetty Kodialbail**[1]

Received: 13 June 2017 / Accepted: 31 October 2017 / Published online: 22 November 2017

Abstract Polyaniline-TiO_2 (PANI-TiO_2) nanocomposite was prepared by in situ polymerisation method. X-ray diffractogram (XRD) showed the formation of PANI-TiO_2 nanocomposite with the average crystallite size of 46 nm containing anatase TiO_2. The PANI-TiO_2 nanocomposite consisted of short-chained fibrous structure of PANI with spherical TiO_2 nanoparticles dispersed at the tips and edge of the fibres. The average hydrodynamic diameter of the nanocomposite was 99.5 nm. The band gap energy was 2.1 eV which showed its ability to absorb light in the visible range. The nanocomposite exhibited better visible light-mediated photocatalytic activity than TiO_2 (Degussa P25) in terms of degradation of Reactive Blue (RB-19) dye. The photocatalysis was favoured under initial acidic pH, and complete degradation of 50 mg/L dye could be achieved at optimum catalyst loading of 1 g/L. The kinetics of degradation followed the Langmuir-Hinshelhood model. PANI-TiO_2 nanocomposite showed almost similar photocatalytic activity under UV and visible light as well as in the solar light which comprises of radiation in both UV and visible light range. Chemical oxygen demand removal of 86% could also be achieved under visible light, confirming that simultaneous mineralization of the dye occurred during photocatalysis. PANI-TiO_2 nanocomposites are promising photocatalysts for the treatment of industrial wastewater containing RB-19 dye.

Keywords Polyaniline-TiO_2 nanocomposite · Reactive Blue (RB-19) · Decolorization · Dye · Kinetics · Photocatalysis

Responsible editor: Suresh Pillai

✉ Vidya Shetty Kodialbail
vidyaks68@yahoo.com; vidyaks95@nitk.ac.in

[1] Department of Chemical Engineering, National Institute of Technology Karnataka, Surathkal, Srinivasnagar Post, Mangalore, Karnataka 575025, India

[2] Department of Chemical Engineering, Manipal Institute of Technology, Manipal, India

Introduction

The industrial processes involving textile dyeing contribute to one of the most environmentally unfriendly processes as they generate coloured wastewater which is densely polluted with dyes, textile auxiliaries along with various chemicals (Golob et al. 2005; Salem et al. 2009). The visibility of the dyes in small quantity is highly significant due to their brilliance (Robinson et al. 2001). In addition, they affect the photosynthetic activity in the aquatic life as they reduce the light penetration (Aksu and Dönmez 2003). As the dyes are chemically and photolytically very stable, they attribute to major concern. They also exhibit low biodegradability. Presence of these dyes in wastewater may also contribute to high chemical oxygen demand (COD) and biochemical oxygen demand (BOD). The process to remove the dyes from wastewater plays a fundamental role in decreasing the impact created by the dye effluents on the environment (Guimarães et al. 2012).

Reactive Blue-19 commonly referred as Remazol brilliant blue is an anthraquinone reactive dye (Fanchiang and Tseng 2009). It is toxic, carcinogenic and mutagenic (Vidhyakalarani and Premaraj 2013). Thus, the wastewater containing these dyes is to be treated before the effluent is discharged into the environment. The conventional methods used for removal of colour from textile effluents include various physical as well as chemical processes namely chemical precipitation, electrocoagulation,

separating the pollutants, coagulation, and elimination by adsorption on activated carbon, etc. (Daneshvar et al. 2003). The conventional methods do not work efficiently as the solubility of synthetic dyes is very high. In addition, most of the commercially produced dyes are designed in such a way as to resist both chemicals as well as biological degradation (Lizama et al. 2002). Thus, there is a need for alternative methods.

Advanced oxidation processes can be described as the process wherein the generation of hydroxyl radicals takes place in sufficient quantities in order to oxidise most of the complex chemicals which are present in the water effluent. Photocatalysis is a type of advanced oxidation process (AOP) (Gogate and Pandit 2004). This process leads to the formation of innocuous products, unlike the classic processes which transfer the pollutants from one medium to another. This process can be employed to destroy a wide range of hazardous compounds in various wastewater sources. In addition, the conditions required for the photocatalytic process are very mild, the time required for the reaction is generally modest and the chemical input is less (Kabra et al. 2004).

For photoreactions to take place, photocatalyst which leads to photon-assisted generation of a catalytically active species is required. When a semiconductor is used as a photocatalyst, initially, a light of certain wavelength is illuminated on its surface. The electrons from the valance band are excited to the conduction band, and holes are left behind in the valence band, provided the energy of the light irradiated is equivalent to the band gap energy. The electrons and the holes undergo oxidation and reduction reactions with the organic pollutants such as dyes which have the possibility to be adsorbed on the surface of the semiconductor (Chatterjee and Dasgupta 2005). The reactions lead to degradation of these organic compounds into simpler compounds, ultimately leading to mineralization.

TiO_2 is an excellent photocatalyst material for water purification owing to its chemical stability, excellent photocatalytic performance, easy availability, lower cost and nontoxic nature. However, major problem possessed by TiO_2 is that it absorbs only in the UV portion of the solar light spectrum. In addition, the probability of recombination of electron (e^-) and hole (h^+) pairs is large. These two problems have been considered as a major technological bottleneck (Wang et al. 2009; Yasmina et al. 2014). Thus, the utilisation efficiency of solar light is limited severely by the wide band gap of TiO_2 (3.2 eV). Recently, the research efforts are in the direction towards improving the utilisation of solar light by extending the photoresponse of TiO_2 to the visible region (Khanna and Shetty 2015). Conducting polymers, such as polyaniline (PANI), have been reported to act as sensitizers in extending the spectral response of TiO_2 to visible region (Mohammadi and Sabbaghi 2014). The spatial separation of charge carrier increases on forming the composite, leading to reduced recombination probability which is relative to that for interfacial charge transfer (Sarmah and Kumar 2011). On irradiation with visible light, PANI absorbs the light which thereby induces π-polaron and polaron-π* transition (Ozbay et al. 2016). The electrons in the excited state of PANI are transported into the d-orbital of TiO_2, as the conduction band or the d-orbital of TiO_2 and the π*-orbital of PANI match very well in the energy level. The electrons get subsequently transferred to the surface, react with water as well as oxygen forming hydroxyl and super peroxide radicals which can oxidise or degrade the dye molecules (Sandhya et al. 2014).

This paper presents the studies on the synthesis of PANI-TIO_2 nanocomposite by in situ polymerisation of aniline along with Degussa P25 (TiO_2) and its photocatalytic activity in terms of degradation of a reactive dye RB-19 under visible light irradiation along with comparison to solar and UV light-mediated photocatalysis.

Methods and materials

Materials

Reactive Blue 19 dyes and aniline were purchased from Sigma-Aldrich Chemicals Pvt. Ltd., Bangalore, India. Hydrochloric acid (HCl) and ammonium peroxodisulphate were purchased from NICE Chemical Pvt. Ltd., Cochin, India. Degussa P 25 was purchased from Intelligent Material Pvt. Ltd., Haryana, India. All the chemicals used were of analytic grade.

Synthesis of polyaniline-TiO_2 nanocomposite

TiO_2 nanoparticles used for the synthesis of PANI-TiO_2 nanocomposite was Degussa P25. The method reported by Radhakrishnan et al. (2009) was adopted for the preparation of PANI-TiO_2 nanocomposite. 0.1 g of TiO_2 nanoparticles were taken in a flask and mixed with 1 mL of aniline and 90 mL of 1 N HCl. A uniform suspension was obtained by ultrasonication for half an hour. One hundred milliliters of pre-cooled 1 N HCl solution containing 2.5 g of ammonium peroxodisulphate was added dropwise to this mixture. The resulting mixture was stirred for 4 h. Ice packs were used to maintain lower temperature during the reaction. The product was then filtered, washed with distilled water and then methanol to remove the impurities. The product was then dried in hot air oven at 100 °C for 12 h.

Characterisation of polyaniline-TiO_2 nanocomposite

The X-ray diffraction (XRD) analysis of the PANI-TiO_2 nanocomposite was carried out by using Rigaku diffractometer under Cu-Kα radiation (1.5406 Å) and shown in Fig. 1. The crystallite size was determined by using Debye Scherrer's formula (Eq. 1).

$$D = K\lambda/\beta\cos(\theta) \quad (1)$$

Where

D crystallite size
K 0.90 Scherrer's constant
λ X-ray wavelength
β the peak width at half-maximum (FWHM)
θ the Bragg diffraction angle

The scanning electron microscopic (SEM) image was recorded by JSM-6380A operated at 20 kV. Fourier transform infrared spectroscopic (FTIR) analysis of the nanocomposite was performed using Bruker Alpha FTIR spectrometer by using KBr pellets. Particle size analysis was performed on a Horiba scientific, nanoparticle analyzer, SZ-100. To determine the band gap energy of the synthesised nanocomposite, the UV-vis spectra of the nanocomposite suspended in distilled water was obtained using Hitachi U-2000 spectrophotometer in a wavelength range of 200 to 800 nm, and the absorbance values were recorded. The band gap energy was calculated using Eq. (2)

$$E = h\frac{c}{\lambda} \quad (2)$$

where E is the band gap energy (eV), h = Plank's constant = 6.626 × 10–34 J s, C = speed of light = 3 × 10^8 m/s and λ is the wavelength (nm).

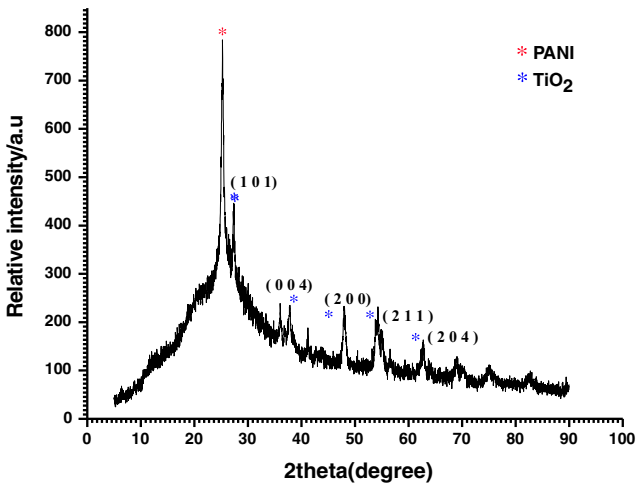

Fig. 1 X-Ray diffraction pattern of PANI/TiO_2 nanocomposite

Photocatalysis for degradation of Reactive Blue-19 under ultraviolet (UV), visible and solar light irradiation

Photocatalytic degradation was carried out in a 250 mL of borosilicate glass beaker placed inside an aluminium chamber (40 cm × 70 cm × 70 cm) equipped with two 18 W UV (Philips) or visible lamps (Polite gold, Mysore Lamps, India). The glass reactor was placed at the centre of the chamber and equidistant from both the lamps. The reactor contents were magnetically stirred, and air was supplied at a rate of 2 LPM continuously during the experiment. An exhaust fan was fitted on top of the chamber, so that a constant temperature was maintained inside the chamber. Solar photocatalysis experiment was performed in open terrace during the month of July from 10.00 AM to 12.00 noon, in the similar reactor set-up without the aluminium enclosure.

Batch experiments for the photocatalytic degradation of RB-19 were carried out using PANI-TiO_2 nanocomposites as photocatalysts under UV, visible and solar light irradiation with 100 mL of 50 mg/L dye solutions. The initial pH of the reaction mixture was adjusted to the required values using either 0.01 N NaOH or 0.01 N H_2SO_4 solutions. The experiments were conducted with a catalyst loading of 1 g/L under constant stirring conditions. Three-milliliter samples were withdrawn at regular intervals over a period of 2 h. The absorbance of the liquid sample at a wavelength of 609 nm was measured using pre-calibrated Hitachi UV-vis spectrophotometer after separating the catalyst from the sample by centrifugation at 12000 rpm for 10 min, and the concentration of Reactive Blue-19 in the solution was then determined. The percentage degradation of the dye was calculated using the formula

$$Degradation(\%) = \frac{(C_{initial} - C)}{C_{initial}} \times 100 \quad (3)$$

where C_{initial} and C are the initial concentration and the concentrations of dye at a particular time in the reactor, respectively. All the experiments on photocatalysis were carried out in duplicates, and the average values with error bars are presented in the plot.

Results and discussion

Characterisation of PANI-TiO_2

Figure 1 shows the XRD pattern of the synthesised nanocomposite. The prominent peaks are exhibited at 2θ = 27.36°, 37.85°, 48.15°, 55.19°, 62.81°, corresponding to anatase TiO_2 (JCPDS NO-01-089-4921) with tetragonal crystal system of different crystalline planes (101), (004), (200) (211),

(204), respectively. However, only one prominent peak at 2θ = 25.1° corresponding to PANI (Pawar et al. 2010) has been exhibited. According to the XRD results and Debye Scherrer's formula, the average crystallite size was found to be 46 nm. The formation of PANI-TiO_2 nanocomposite was confirmed by the XRD analysis. The SEM image of PANI-TiO_2 nanocomposite shown in Fig. 2 exhibits short-chained fibrous structure of PANI with spherical TiO_2 nanoparticles dispersed at the tips and edge of the fibrous matrix of PANI. Huyen et al. (2011) have also observed such PANI chains with dispersed TiO_2 particles in the nanocomposites. The nanocomposite appears to be porous structured. Formation of porous PANI-TiO_2 nanocomposite has also been reported by Asha et al. (2015).

Figure 3a, b and c shows the TEM images of the PANI-TiO_2 nanocomposites at different magnifications. The fibrous structure of PANI is confirmed in the TEM images shown in Fig. 3a and the presence of dispersed spherical TiO_2 nanoparticles at the tips and edges of the fibrous structure of PANI. As shown in Fig. 3a, b, tubular PANI particles are long and entangled with an average width of around 45 nm. Spherical TiO_2 nanoparticles were observed on the surface of the PANI tubule and are of average size of around 19.6 nm. Ansari et al. (2014) and Huyen et al. (2011) have also observed TiO_2 particles scattered at the tips of the PANI. Figure 3c shows the TEM image of a single TiO_2 particle which reveals a well-ordered crystal lattice structure indicating a high degree of crystallinity of TiO_2. Ansari et al. (2015) have also observed highly crystalline TiO_2 particles on the tips of PANI.

Figure 4 shows the size distribution of the particles as obtained by dynamic light scattering (DLS) technique with deionised water as the solvent. The size distribution is in a narrow range which represented the formation of uniform-sized particles. The average hydrodynamic diameter of the nanocomposite is 99.5 nm.

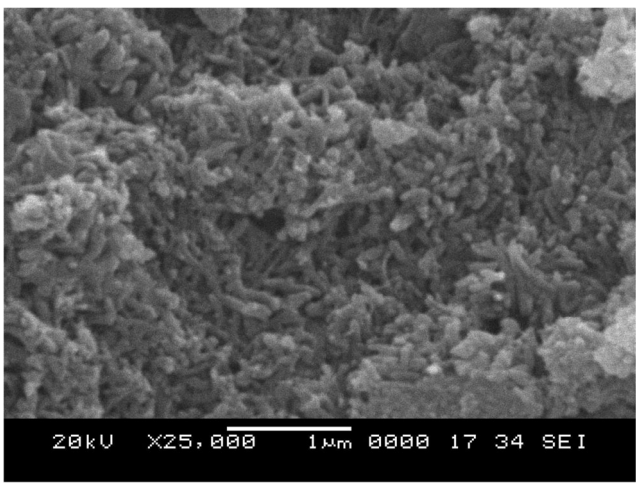

Fig. 2 Scanning electron microscope of PANI-TiO_2 nanocomposite

Figure 5 shows the FTIR spectra of the PANI-TiO_2 nanocomposite. The low wave number region exhibits a strong vibration around 500 cm^{-1}, which corresponds to the antisymmetric Ti-O-Ti mode of the titanium oxide (Al-Daghman et al. 2015). The 1200 cm^{-1} band is associated with the C–N stretching mode for benzenoid ring typical of PANI (Guo et al. 2012). The peak at 1400 cm^{-1} can be attributed to ring-stretching of the phenazine constitutional units (Trchová and Stejskal 2011). The substituted phenazine constitutional units can be formed by the oxidative intermolecular cyclization or insertion of aniline molecules into ortho or para positions of the constitutional units (Trchová et al. 2006; Trchová and Stejskal 2011). The bands at 1500 and 1600 cm^{-1} are attributed to the C = N and C = C stretching mode of vibration for the quinoid and benzenoid ring units of PANI (Pawar et al. 2010; Guo et al. 2012). The vibration bands at 3400 cm^{-1} are caused by the NH stretching of secondary amines (Nabid et al. 2008). The FTIR results confirmed the formation of PANI –TiO_2 composite.

The absorption spectrum of TiO2, PANI and PANI-TiO_2 nanocomposite was obtained using UV-vis spectrophotometer and is shown in Fig. 6a. As observed from Fig. 6a, TiO_2 shows an absorption peak at 275 nm, and the absorbance values decreased to a minimum under visible light wavelength range, showing that maximum absorption occurs in the UV range for TiO_2 and the absorption under visible light wavelength range is minimal. However, the absorbance for PANI or PANI-TiO_2 is low at wavelengths lesser than 315 nm. Three absorption peaks are observed for PANI at 305, 365 and at 436 nm. The first two peaks in the UV region are attributed to π-π* transition of benzenoid ring. The third peak in the visible region is attributed to polaron-π* transition of PANI (Stejskal et al. 1993; Xia et al. 1995; Radoičić et al. 2012). Three peaks have also been observed for PANI-TiO_2 nanocomposites, with no shift in the first and second peak after compositing with TiO_2. However, a red shift in the third peak has occurred with the peak at 446 nm for PANI-TiO_2 nanocomposites, which is owing to coordination of TiO_2 with the nitrogen atom of PANI and permitted interaction with each other via π conjugated system (Ansari et al. 2014). Kohut-Svelko et al. (2005) have reported that the interaction of TiO_2 with PANI chains may contribute to the presence of deprotonated PANI segments resulting in the peak shift. According to them, the peak shift may also occur because of the presence of significant amount of structural defects in the PANI part of the nanocomposites which may boost the winding between aromatic rings, changing electronic structure leading to increased polaron localization, and to the condensed conjugation length of chains.

Further increase in wavelength in the visible range slightly reduced the absorbance value with minimum absorbance at around 550 nm for PANI-TiO_2 and at 525 nm for PANI. However, appreciable absorbance has been observed in the

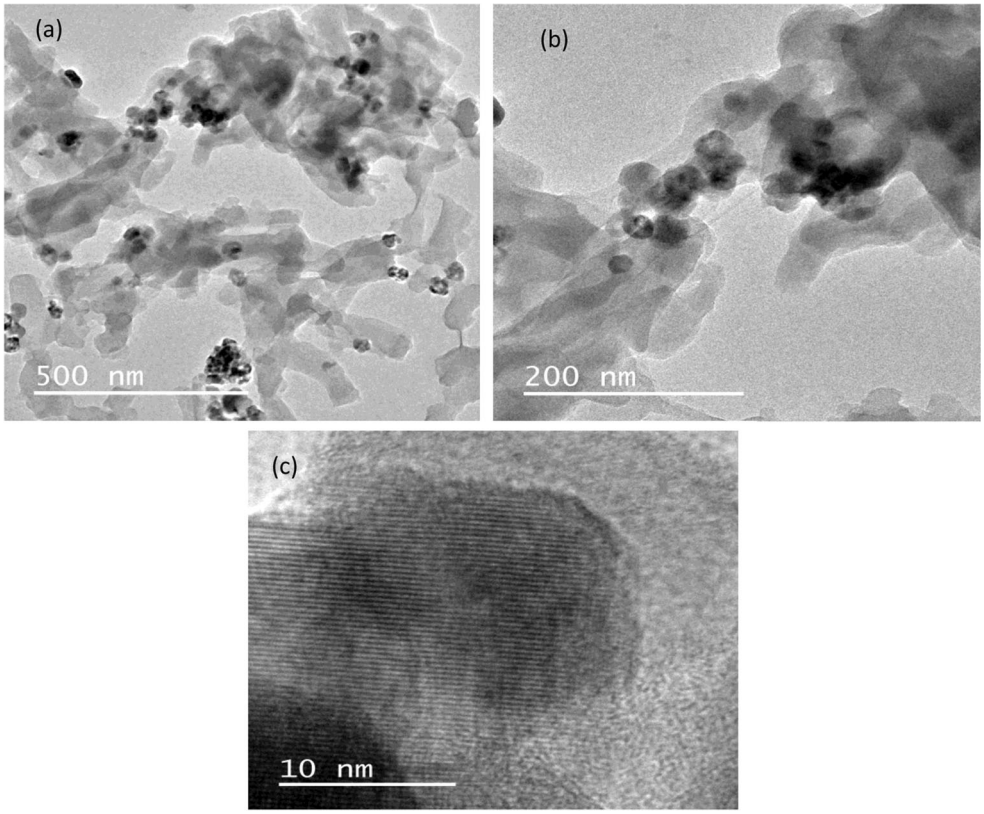

Fig. 3 Transmission electron microscope PANI-TiO_2 nanocomposite, image (**a** and **b**) hexagonal TiO_2 nanoparticles were observed on the edges of the PANI tubule (**c**) highly crystalline TiO_2 nanoparticle on the edges on the PANI

entire visible range up to 700 nm both with PANI and PANI-TiO_2. The absorbance values for PANI are lower than that for PANI-TiO_2 showing superior light absorption performance of PANI-TiO_2. PANI-TiO_2 nanocomposites are able to absorb light in both UV and visible range, thus indicating its potential use as a photocatalyst both under UV and visible light. The PANI-TiO_2 nanocomposites can be activated by UV and visible light concurrently. This feature is advantageous for good photocatalytic activity under solar light which comprises of UV and visible light radiations.

To determine the band gap energy for PANI-TiO_2, Tauc's plot of $(hcA/\lambda)^2$ vs. (hc/λ) was plotted which exhibited a linear region as shown in Fig. 6b indicating direct allowed transition. The extrapolation of the linear region of Tauc's plot intersecting the *x*-axis gives the value of the optical band gap energy, *E*. The calculated value of band gap energy of PANI-TiO_2 is 2.1 eV which corresponds to a cut off wavelengths of 563 nm. The band gap energy of the PANI-TiO_2 nanocomposite is much lower than that of TiO_2 which has a band gap energy value of 3.2 eV (Hidalgo et al. 2015). It confirms the

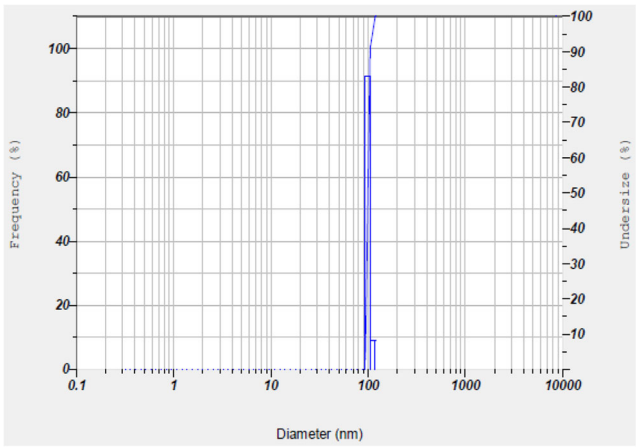

Fig. 4 Size distribution of PANI-TiO_2 nanocomposite measured by the DLS technique

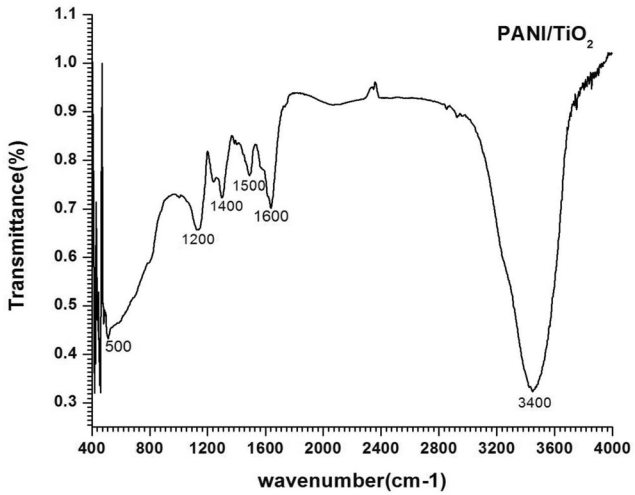

Fig. 5 FTIR spectra of PANI-TiO_2 nanocomposite

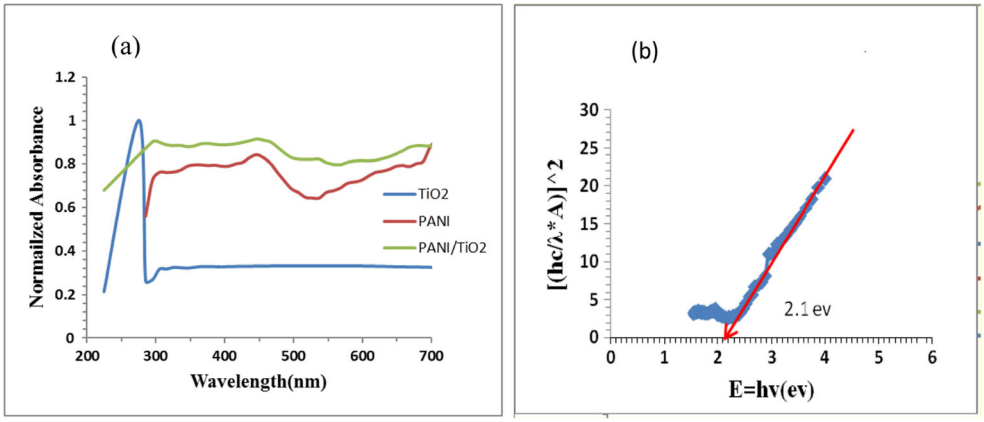

Fig. 6 **a** UV-visible spectra of TiO_2, PANI, and PANI-TiO_2 nanocomposite. **b** Tauc plot for the determination of band gap of PANI-TiO_2 nanocomposite

potential of the nanocomposite for its application as a visible light active photocatalyst.

Photocatalytic activity of PANI-TiO_2 nanocomposite under visible light irradiation

The efficacy of *PANI-TiO_2 nanocomposite* as a photocatalyst in degradation of RB-19 dye under visible light irradiation was studied with initial concentration of dye at 50 mg/L and catalyst loading of 1 g/L and under initial pH of 7.1 (unadjusted). Figure 7 shows that the percentage dye degradation in the absence of catalyst and on irradiation with visible light is very minimal (less than 13% in 120 min) as compared to that in the presence of catalyst on irradiation with visible light. The effect of the light irradiation in the absence of catalyst was negligible, confirming a small effect of photolytic removal of the dye by visible light irradiation. 91.84% of 50 mg/L of RB-19 dye could be degraded within 60 min, and complete degradation occurred in 120 min of irradiation in the presence of 1 g/L PANI-TiO_2 nanocomposite, whereas only around 40% degradation was achieved with Degussa P25. It confirmed that

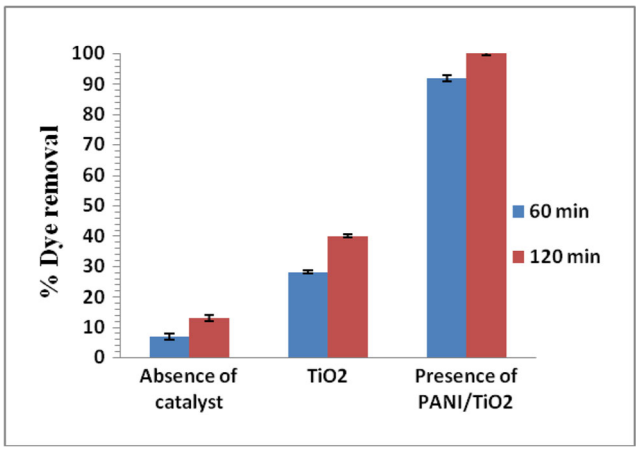

Fig. 7 Percentage degradation of RB-19 dye for irradiation time of 60 and 120 min in the presence of PANI-TiO_2 nanocomposites, TiO_2 and in the absence of photocatalyst under visible light irradiation (conditions: dye concentration = 50 mg/L, catalyst loading = 1 g/L)

PANI-TiO_2 nanocomposite is an effective visible light active photocatalyst in the degradation of RB-19 dye and it exhibits superior performance in comparison to Degussa P25. As observed in Fig. 6, PANI-TiO_2 can absorb light significantly in the entire visible light wavelength range and has band gap energy of 2.1 eV which is much lower than that of TiO_2. Thus, it showed considerably a better photocatalytic activity as compared to TiO_2. Figure 6a showed a maximum absorbance for TiO_2 at 275 nm and very low absorption in the longer wavelength range, which is owing to its high band gap energy of greater than 3.2 eV. The electron–hole recombination rate for TiO_2 may be much higher than that of PANI-TiO_2. Thus, TiO_2 showed a very low activity in visible light wavelength range.

Effect of pH on the photocatalytic degradation of RB-19 under visible light irradiation

Strong adsorption of the molecules to be degraded on the solid catalyst is usually regarded as a prerequisite for their effective photocatalytic degradation (Alkaim et al. 2013). pH of the solution affects the charge on the catalyst and the dissociation of the species present in the compounds to be oxidised (Yasmina et al. 2014). Thus, pH strongly influences the adsorption of the molecules on the surface of the photocatalyst.

To study the effect of pH, the experiments were conducted with initial dye concentration of 50 mg/L and with 1 g/L of PANI-TiO_2 nanocomposites loading at different initial pH conditions. Figure 8 presents the percentage degradation of RB-19 dye during irradiation under visible light at initial pH of 3, 5, 6, 7.1 (unadjusted) and 9. As shown in Fig. 8, after 120 min of irradiation, complete degradation has been achieved at pH 3. Though the degradation at 120 min of irradiation was around 98% at pH 5 to 7, only around 85% degradation could be achieved at alkaline pH 9. The effect of pH is evident from the comparison of the percentage degradation of the dye after 60 min of irradiation time. It is observed that the percentage degradation decreased as the initial pH was increased from acidic to near neutral (unadjusted) and then

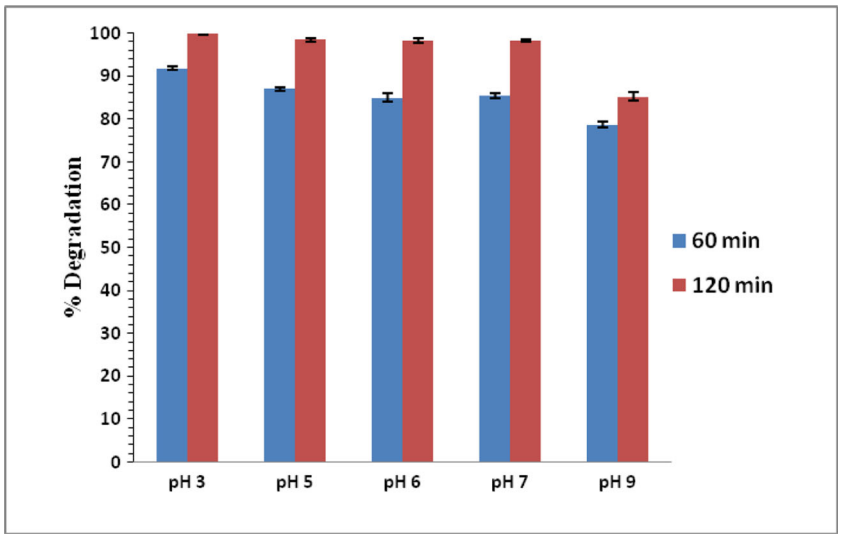

Fig. 8 Percentage degradation of RB-19 after irradiation time of 60 and 120 min at different initial pH conditions under visible light irradiation. Conditions: dye concentration = 50 mg/L, catalyst loading = 1 g/l

to alkaline conditions revealing that the rate of degradation is high at acidic pH and reduces with increase in pH. Thus, acidic pH is found to be favourable. When the pH is maintained at acidic conditions, the surface charge on the catalyst is positive and there occurs an electrostatic attraction between the negatively charged anions of RB-19 dyes and the surface of the catalyst. It favours the adsorption of the dye on the catalyst. Adsorption of the dye onto the catalyst in turn favours the photocatalysis. On the contrary, when the pH is maintained at 9, the surface charge on the catalyst is negative and there occurs an electrostatic repulsion between the Reactive Blue-19 dye and the catalyst. Hence, the favourable pH value for the photocatalytic degradation of RB-19 over PANI-TiO_2 was found to be 3.

Effect of catalyst loading on the photocatalytic degradation of RB19 under visible light irradiation

The photocatalytic rate at which photocatalysis takes place is a function of catalyst loading (Shet and Shetty 2016). Optimum catalyst loading has to be determined to ensure total absorption of photons (Priya et al. 2015) and to minimise the cost of operation by preventing the excess usage of catalyst. Batch photocatalysis was conducted at different catalyst loadings of 0.5, 1, 2 and 2.5 g/L with an initial dye concentration of 50 mg/L and at initial pH 3. The percentage degradation at 120 min of irradiation by visible light with PANI-TiO_2 nanocomposites is shown in the Fig. 9. As the concentration of the catalyst increased from 0.5 to 1 g/L, the percentage degradation increased from 93.5% to almost complete degradation. This can be attributed to the fact that the total active surface area of the catalyst increases with the increase in catalyst loading (Chen et al. 2011) which increases the number of surface active sites available for photocatalytic reaction. Comparison of the percentage degradation at 60 min also shows that the degradation is slower at catalyst loading of 0.5 g/L yielding only around 77% and increases significantly with increase in loading to 1 g/L. However, further increase in catalyst loading above 1 g/L has marginally reduced the degradation. As the catalyst loading was increased further, the percentage degradation decreased reaching around 93.5% (after 120 min) with catalyst loading of 2.5 g/L. The decrease is due to the increase in the opacity of the solution with higher catalyst loading which decreases the penetration of photon flux in the reactor and thereby decreasing the photocatalytic rate (Kamble et al. 2003). Thus, catalyst loading of 1 g/L is the optimum for the degradation of 50 mg/L of RB-19 dye under the conditions studied.

Effect of dye concentration on the photocatalytic degradation of RB-19 under visible light irradiation

The industrial effluents may contain dye at different concentration. Dye concentration affects the rate of photocatalytic process. Thus, the effect of initial dye concentration was studied. Batch photocatalysis experiments were conducted at different dye loadings of 50, 75, 100 and 125 mg/L with the PANI-TiO_2 nanocomposite loading of 1 g/L and at initial pH 3. The percentage degradation at 60 and 120 min of irradiation by visible light is shown in Fig. 10. As the dye concentration increased from 50 to 125 mg/L, the percentage degradation decreased from 100 to 71% degradation at 120 min irradiation under visible light. Comparison of the percentage degradation at 60 min also shows that the degradation decreases with increase in dye concentration. This might be due to the elevated optical density at higher concentrations (Reutergådh and Iangphasuk 1997; Matthews 1991) hindering the photon transfer through the medium (Reutergådh and Iangphasuk 1997; Matthews 1991). As the dye concentration increases, the obstruction of light penetration in solution causes reduced photocatalysis (Mozia et al. 2009; Kumar et al. 2016). The

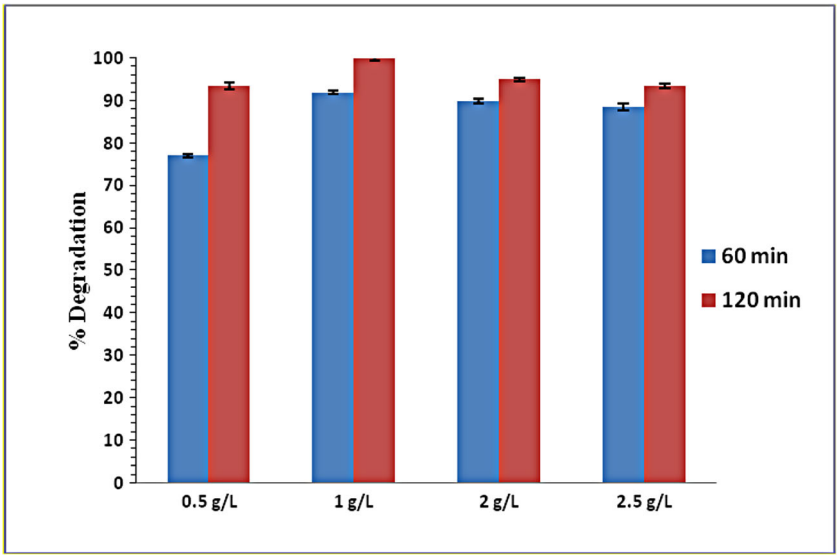

Fig. 9 Percentage degradation of RB-19 after irradiation time of 60 and 120 min at different catalyst lording under visible irradiation. Conditions: dye concentration = 50 mg/L; pH = 3

catalyst loading of 1 g/L may be sufficient enough to cause almost complete degradation of 50 mg/L dye loading in 120 min. However, increase in dye concentration would lead to crowding of the dye molecules on the available active sites for adsorption. The percentage of successful collisions causing dye adsorption reduces with an increase in dye concentration, thus resulting in reduced rate of degradation. Thus, longer time may be required for complete degradation of higher concentrations of the dye.

Comparison of visible light-induced photocatalytic activity of PANI-TiO_2 nanocomposite with UV and solar light activity

To study the effect of light source, experiments were carried out under natural sun light, artificial visible and UV light irradiation with an initial dye concentration of 50 mg/L and catalyst loading of 1 g/L with initial pH 3. Figure 11 shows the percentage dye removal under UV, visible and solar light irradiation. As observed in Fig. 11, almost complete degradation of RB-19 dye could be achieved in 120 min of irradiation time under visible and solar light, whereas under UV light around 98.4% was achieved. It is observed that the rate of photocatalytic degradation is marginally faster under solar irradiation followed by visible and then by UV irradiation as observed from the degradation at 60 min irradiation. The dye removal was less than 8% under dark conditions in the presence of catalyst as compared to that under light, indicating that dye removal by permanent adsorption is minimal. Thus, it is confirmed that PANI-TiO_2 nanocomposite acts as a photocatalyst in the degradation of dyes, and the rate of dye removal is very fast. The reactive species $*O_2^-$ and *OH are formed due to the illumination of the catalyst. These reactive species attack the azo bond of RB-19 which cause the cleavage of the azo bond and thereby lead to the decolourisation of dye solution (Khanna and Shetty 2014).

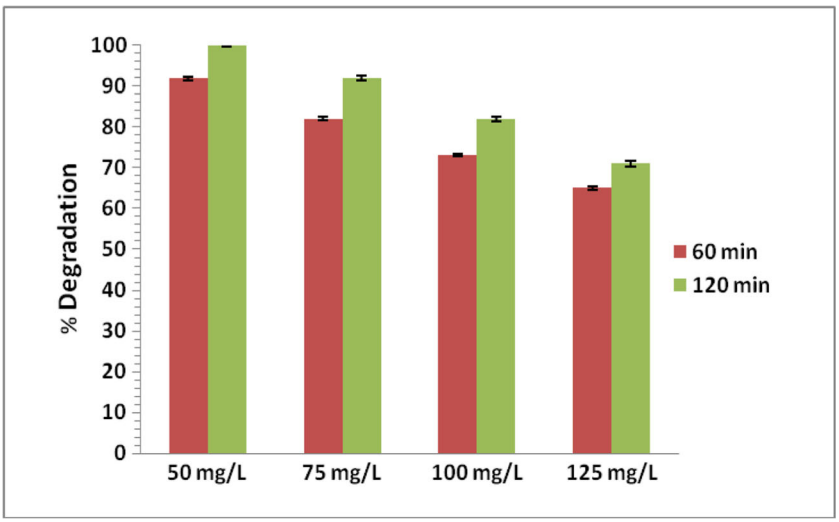

Fig. 10 Percentage degradation of RB-19 after irradiation time of 60 and 120 min at different initial dye concentrations under visible light irradiation. Conditions: catalyst concentration = 1 g/L; pH = 3

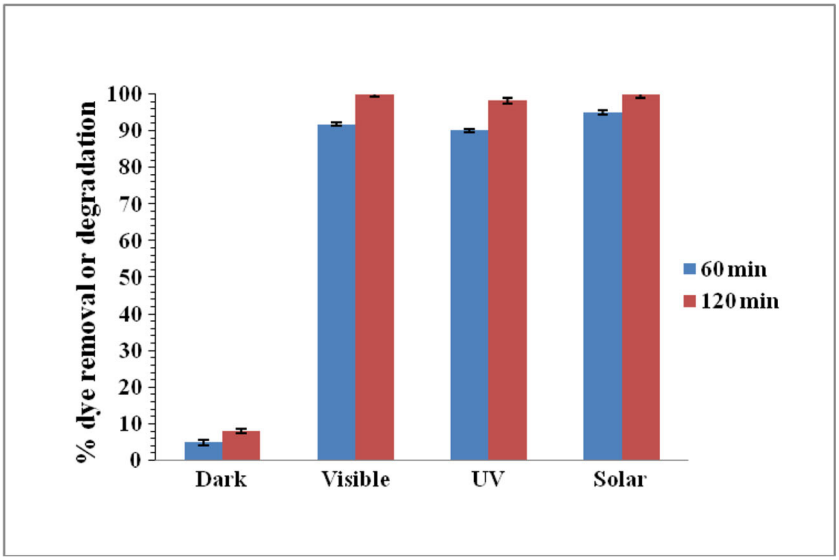

Fig. 11 Percentage degradation of RB-19 under different source of light after irradiation time of 60 and 120 min. Conditions: dye concentration = 50 mg/L; catalyst loading of 1 g/L; pH = 3

The high photocatalytic efficiency is exhibited under all the three light sources, which might be due to the low band gap energy of PANI-TiO_2 nanocomposite. As can be observed from the absorbance spectra for PANI-TiO_2 nanocomposite in Fig. 6a, it has appreciable absorbance in the wavelength range from 300 to 700 nm, showing its capability to absorb the light in both UV and visible light range. Thus, it shows almost similar activity under UV and visible light as well as in the solar light which comprises of radiation in both UV and visible light range.

These results show that PANI-TiO_2 nanocomposites are very active photocatalysts and can be used for wastewater treatment to degrade the dyes under visible and solar lights in regions where solar light is abundantly available. However, artificial UV or visible light irradiation can be adopted for the photocatalytic water treatment when solar light is not available.

Figure 12a shows the proposed mechanism of photodegradation of RB-19 dye by PANI-TiO_2 nanocomposite under visible light irradiation. PANI particles attract photons at their edge under irradiation. The charge transferred immediately from the highest occupied molecular orbital (HOMO) to the lowest unoccupied molecular orbital (LUMO) of PANI (Reddy et al. 2010). The photogenerated electrons are transferred from LUMO to the conduction band (CB) of TiO_2, to form electron centre (Zhang et al. 2006; Li et al. 2008). At the same time, the transitions between π-polaron and polaron-π * in PANI molecules can be induced (Xia et al. 1995). The photogenerated holes in the π orbital of PANI can migrate to the interface and react with water to give up hydroxyl radicals. This would significantly help in charge separation and to reduce the charge recombination. In this case, PANI acts as a photo sensitizer. Excited-condition electrons from the PANI molecules can be injected into the conduction band of TiO_2 and eventually react with oxygen at the surface. This result in the configuration of highly reactive particles, such as the superoxide radical ion O_2• and as a result the hydroxyl radical OH•, which are responsible for the degradation of the organic compound (Yu et al. 2011; Zhang et al. 2006; Elsayed and Gobara 2016).

Therefore, the superior photocatalytic activity of PANI-TiO_2 as compared to TiO_2 nanoparticles is owing to quick charge separation and slow charge recombination. The improved visible light absorption of PANI-TiO_2 nanocomposite is not the only reason that induces increased photocatalytic activity, but also owing to reduced electron-hole recombination rate (Radoičić et al. 2013).

Figure 12b shows the proposed mechanism of photodegradation of RB-19 dye by PANI-TiO_2 nanocomposite under UV light irradiation. Under UV irradiation, both PANI and TiO_2 in the nanoparticles attract photons at their edges; immediately, the charge is transferred from HOMO to LUMO of PANI (Reddy et al. 2010). As observed in Fig. 6a, PANI absorbs light appreciably in the wavelengths greater than 300 nm. This shows that PANI is also excited under UV light in the range from 300 to 400 nm. TiO_2 is excited by UV light leading to separation of electron and holes. The first two peaks in the UV region at 305 and 365 nm are attributed to π-π* transition of benzenoid ring of PANI (Stejskal et al. 1993; Xia et al. 1995; Radoičić et al. 2012). The photogenerated electrons are transferred from LUMO of PANI to the CB of TiO_2, to form electron centre (Zhang et al. 2006; Li et al. 2008; Reddy et al. 2010), thus enhancing the charge separation and formation of superoxide radicals, in the presence of O_2. These radicals further react with water producing OH• radicals (Li et al. 2008; Zhang et al. 2008; Reddy et al. 2010). The photogenerated holes in TiO_2 nanoparticles travel to the HOMO of PANI to form hole centre. The

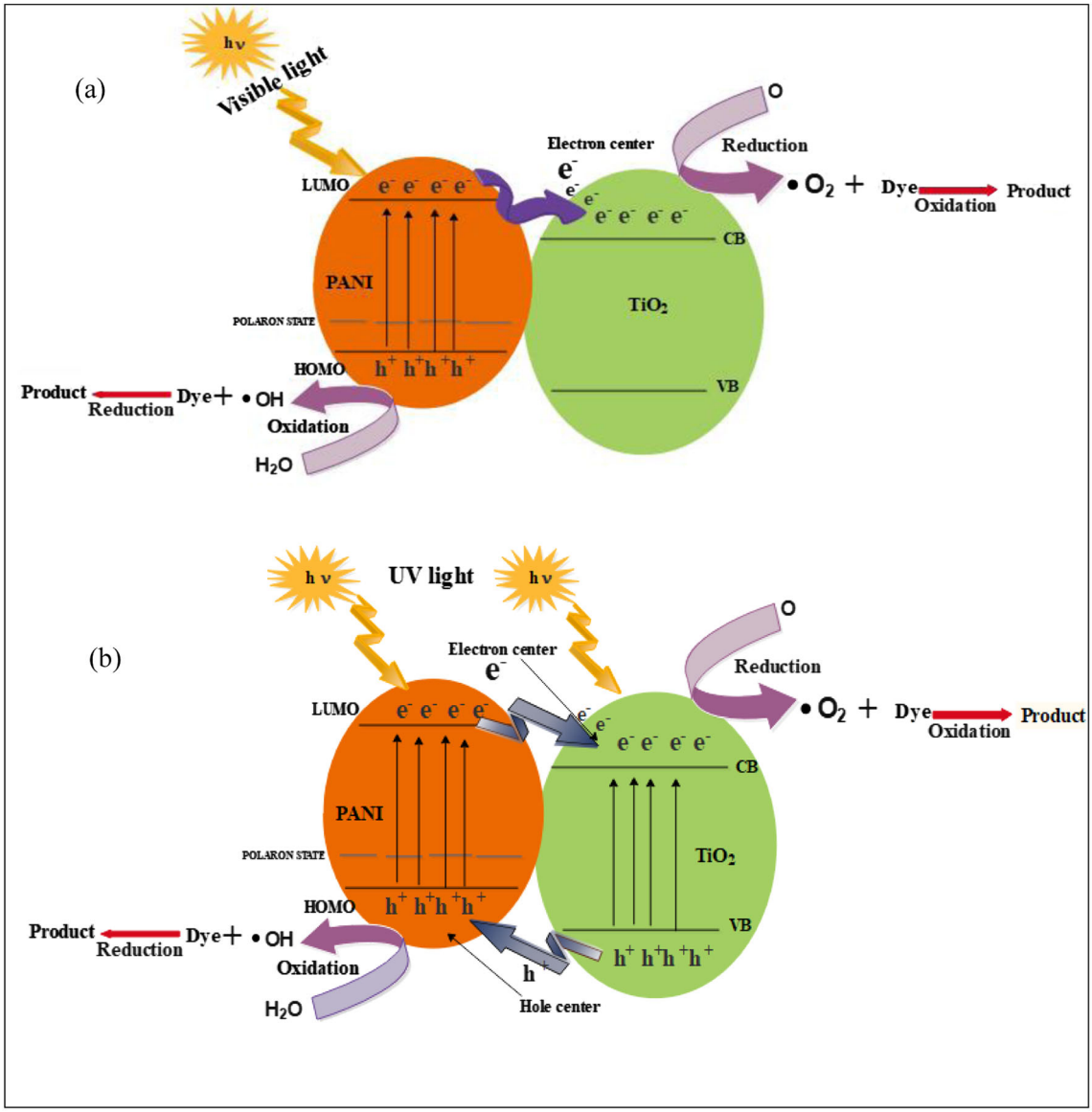

Fig. 12 Proposed mechanism of photocatalytic degradation of dye under (**a**) visible light and (**b**) UV light by PANI-TiO_2 nanocomposite

holes from PANI species are released from hole centres on adsorption of H_2O molecule onto the surface of the photocatalyst, and bringing about the oxidation of H_2O to •OH, which further leads to reduction of the dye molecules. On the other hand, based on the position of redox potentials (Li et al. 2006; Yue et al. 1991; Senadeera et al. 2004), the holes generated in the valence band of TiO_2 can also drift to the orbital of PANI and create a contribution to the oxidation of adsorbed dye molecules (Li et al. 2008; Zhang et al. 2008). Thus, under UV light irradiation, photons are absorbed both by PANI and TiO_2 (Radoičić et al. 2013), thus leading to the formation of hole centres in PANI and electron centres in TiO_2 which aid charge separation and in lowering the charge recombination rate both in PANI and TiO_2. Thus, PANI-TiO_2 nanocomposite shows a considerable photocatalytic activity under UV light.

Kinetics of degradation of RB-19 using PANI-TiO_2 nanocomposite under visible light irradiation and comparison with the kinetics under solar and UV light

Studies on kinetics of degradation of the dye are important in the design of photocatalytic reactors used for industrial wastewater treatment applications. The estimation of the rate equation and the determination of the rate equation parameters are important in kinetics (Khanna and Shetty 2014). Kinetics of photocatalytic degradation of RB-19 under visible light, solar light and UV light irradiation at a catalyst loading 1 g/L and initial pH 3 were studied. The kinetic data was obtained by batch experiments conducted with initial RB-19 concentration of 50 mg/L. Heterogeneous photocatalysis rate generally follows the Langmuir-Hinshelwood kinetic model

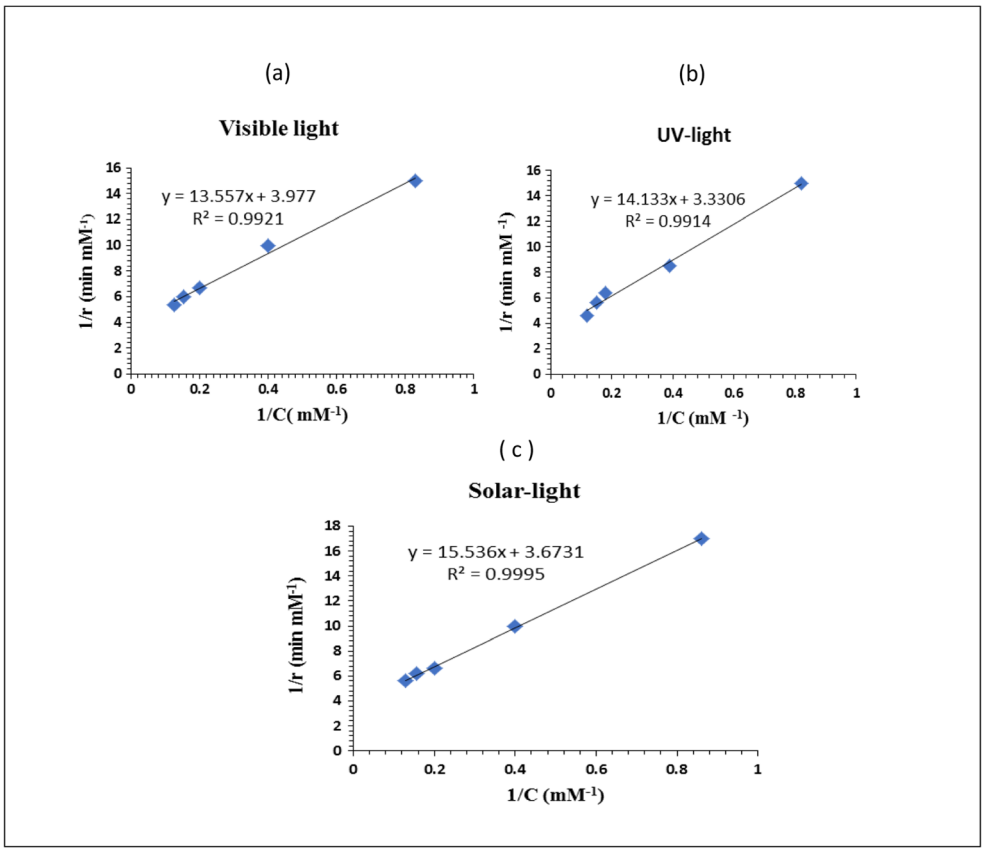

Fig. 13 L-H model fit for the rate kinetics of photocatalytic degradation of RB-19 dye by PANI-TiO_2 under UV (**a**), visible (**b**) and solar light (**c**) irradiation with catalyst loading of 1 g/L and pH 3

(Ahmad and Mondal 2012; Khanna and Shetty 2014), shown as Eq. (3).

$$r = \frac{kK_eC}{1 + K_eC} \tag{3}$$

where r is the rate of degradation of the dye in millimolar per minute, C is the dye concentration in millimolar. Here, k indicates the limiting rate of the reaction at maximum coverage under the given experimental conditions while K_e represents the equilibrium constant for adsorption of dye on the illuminated PANI-TIO_2 surface (Sauer et al. 2002).

In the present study, L-H kinetic model was tested for its validity. The rate of degradation of Reactive Blue-19 was determined from the experimental concentration-time data. The linear form of the model is shown as Eq. (4)

$$\frac{1}{r} = \frac{1}{kK_e}\frac{1}{C} + \frac{1}{k} \tag{4}$$

1/r v/s 1/C for UV, visible and solar photocatalysis were plotted and are shown in Fig. 13. The plots are linear with coefficient of determination (R^2) value very near to one, indicating that the kinetics of photocatalytic degradation of RB-19 dye under UV, visible and solar irradiation by PANI-TiO_2 nanocomposites, obey the Langmuir-Hinshelwood kinetic model. Table 1 presents the values of k and K_e of the kinetic model for the degradation of dye under UV, visible and solar irradiation. Applicability of L-H kinetic equation shows that the photocatalysis of dye by PANI-TiO_2 nanocomposite is an adsorption controlled process.

Dye mineralization by photocatalysis using PANI-TiO_2 nanocomposite under visible light irradiation

The dye may be degraded to form certain intermediates during the oxidation and some of them might be more toxic than the parent compounds. As a result, it is essential to understand the mineralization of the dye (Medien and Khalil 2010). Mineralization accounts for the oxidation of the dye into CO_2, water and other simpler compounds. Chemical oxygen demand (COD) is the most frequently used parameter in assessing the pollution level in wastewater and it is used as a

Table 1 Values of k and K_e for degradation of kinetics for AY-17 and RB-19 under solar light

Rate parameter	UV	Visible	Solar
k (mM min^{-1})	0.300	0.251	0.272
K_e (mM^{-1})	0.236	0.294	0.237

parameter to show the extent of dye mineralization. The COD of water contaminated with the dye was measured at regular intervals during photocatalytic reaction to confirm the degradation of dyes into simpler compounds. The percentage of COD removal (mg/L) during photocatalysis is shown in Fig. 14. The COD levels decreased from initial 1400 to 200 mg/L after 120 min of irradiation. The reduction in oxygen demand during the improvement of reaction confirms the degradation of the dye during the photocatalytic process (Ejhieh and Shamsabadi 2013). Around 86% removal of COD could be achieved in 120 min of irradiation by photocatalysis of 50 mg/L dye. This result indicates that PANI-TiO_2 nanocomposites are efficient photocatalysts under visible light irradiation and mineralization of the dye in wastewater progresses during photocatalysis along with decolourization.

Table 2 shows the degradation of RB-19 by various methods as reported in literature. On comparison of the degradation achieved, the present method shows almost complete degradation of the dye in 120 min under visible light and around 98.4% degradation under UV light. Around 86% COD removal could also be achieved under visible light, confirming the simultaneous mineralization of the dye. The photocatalyst is visible light active and can be used for treatment of the dye-contaminated water under solar light or visible light. The process does not involve the use of oxidants such as H_2O_2 or any other reagents like Fenton reagent. It does not involve the application of ultrasound energy; the process involves no use of chemicals and allows harnessing natural sunlight for wastewater treatment. The process also aids in mineralization of the dye, thus ensuring the reduction of pollution load into the environment. Thus, the photocatalysis of RB-19 using PANI-TiO_2 is a favourable process.

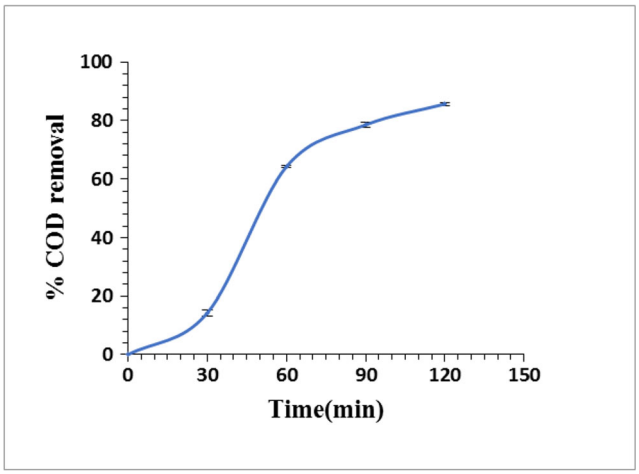

Fig. 14 COD removal from degradation of RB-19 dye by PANI-TiO_2 under visible light irradiation with catalyst loading of 1 g/L and pH 3

Table 2 RB-19 degradation by various methods

Process	Catalyst/catalyst loading	Other specific conditions	Light source	Percentage degradation	Reference
Photolysis	Not applicable	H_2O_2 oxidant (2.5 mM)	UV	90% of 100 mg/L dye in 180 min	Rezaee et al. 2008
Photocatalysis	TiO2 nanofiber/1 g/L loading	H_2O_2 oxidant	UV light	Complete dye removal and 45% COD removal from 25 mg/L dye in 5 h	Rezaee et al. 2009
UV/H2O2	–	500 mg/L H_2O_2	UV	91% degradation of 100 mg/L dyes in 3 h	Guimarães et al. 2012
Photo Fenton process	–	150 mg/L H_2O_2 and 15 mg/L Fe^{2+}	UV	> 94.5% dissolved organic carbon and 99.4% colour removal from 100 mg/L dye in 60 min	Guimarães et al. 2012
Photocatalysis	TiO_2-clay composite/0.5 g/L loading	H_2O_2	UV	Complete degradation of 75 mg/L in 25 min	Hadjltaief et al. 2014
Photocatalysis	Sulphur-doped TiO_2 catalyst loading/5 wt% loading	–	Visible light	73% of 20 mg/L dye	Khan et al. 2015
Photo-sono catalysis	Sulphur-doped TiO_2 Catalyst/5 wt% loading	100 Hz ultrasound	Visible light	90% of 20 mg/L dye	Khan et al. 2015
Photocatalysis	PANI-TiO_2 nanocomposite/1 g/L	–	Visible light and solar light	Complete degradation of 50 mg/L dye in 120 min and 86% COD removal under visible light	Present work
Photocatalysis	PANI-TiO_2 nanocomposite/1 g/L	–	UV light	98.4% in 120 min	Present work

Conclusion

PANI-TIO_2 nanocomposite synthesised by in situ polymerisation of aniline along with Degussa P25 (TiO_2) was characterised and found to have an average crystallite size of 46 nm, hydrodynamic diameter of 99.5 nm with vary narrow size distribution indicating uniform-sized particles. FTIR results confirmed the formation of PANI-TIO_2 nanocomposite. PANI-TIO_2 nanocomposite contained short-chain fibrous PANI structure with spherical TiO_2 nanoparticles dispersed on the edge and tips. The band gap energy value of 2.1 eV showed its potential as a good visible light active photocatalyst. These nanoparticles have shown visible light-mediated photocatalytic activity in terms of degradation of RB-19 dye. The visible light active photocatalytic degradation of RB-19 follows the Langmuir-Hinshelwood kinetic model with $k = 0.251$ mM $min^{-1}$and $K_e = 0.294$ mM^{-1}. The photocatalytic activity under solar light was similar as that under visible light and marginally superior to that under UV light. Fifty milligrams per liter of RB-19 dye undergoes complete degradation within a time span of 120 min at acidic pH of 3 and with catalyst loading of 1 g/L both under visible light and solar light irradiation. As the dye concentration increased from 50 to 125 mg/L, the percentage degradation decreased from 100 to 71%. COD removal of around 86% could be achieved under visible light with 50 mg/L dye indicating the mineralization of the dye. Owing to the ability of PANI-TiO_2 nanocomposite to absorb light both in UV and visible range, the photocatalyst can serve under solar light. Thus, solar photocatalysis with PANI-TIO_2 nanocomposite can be used for the treatment of RB-19 dye-contaminated water owing to faster photocatalytic degradation with increased efficiency along with benefits of very low power inputs and cost effectiveness.

References

Ahmad R, Mondal PK (2012) Adsorption and photodegradation of methylene blue by using PANI/TiO_2 nanocomposite. J Dispers Sci Technol 33:380–386

Aksu Z, Dönmez G (2003) A comparative study on the biosorption characteristics of some yeasts for Remazol blue reactive dye. Chemosphere 50:1075–1083

Al-Daghman AN, Ibrahim K, Ahmed NM, Zaidan KM (2015) Effect of TiO_2 thin film morphology on polyaniline/TiO_2 solar cell efficiency. World J Nano sci Eng 5:41–48

Alkaim AF, Kandiel TA, Hussein FH, Dillert R, Bahnemann DW (2013) Enhancing the photocatalytic activity of TiO_2 by pH control: a case study for the degradation of EDTA. Catal Sci Technol 3:3216–3222

Ansari MO, Khan MM, Ansari SA, Lee J, Cho MH (2014) Enhanced thermoelectric behaviour and visible light activity of Ag@ TiO_2/polyaniline nanocomposite synthesized by biogenic-chemical route. RSC Adv 4:23713–23719

Ansari MO, Khan MM, Ansari SA, Cho MH (2015) Electrically conductive polyaniline sensitized defective-TiO_2 for improved visible light photocatalytic and photo electrochemical performance: a synergistic effect. New J Chem 39:8381–8388

Asha A, Goyal SL, Kumar D, Kumar S, Kishore N (2015) Synthesis and characterization of polyaniline/TiO_2 composites. Indian J Pure Appl Phys 52:341–347

Chatterjee D, Dasgupta S (2005) Visible light induced photocatalytic degradation of organic pollutants. J Photochem Photobiol C: Photochem Rev 6:186–205

Chen C, Liu J, Liu P, Yu B (2011) Investigation of photocatalytic degradation of methyl orange by using nano-sized ZnO catalysts. Adv Chem Eng Sci 1:9–14

Daneshvar N, Salari D, Khataee AR (2003) Photocatalytic degradation of azo dye acid red 14 in water: investigation of the effect of operational parameters. J Photochem Photobiol 157:111–116

Ejhieh AN, Shamsabadi MK (2013) Decolorization of a binary azo dyes mixture using CuO incorporated nanozeolite-X as a heterogeneous catalyst and solar irradiation. Chem Eng J 228:631–641

Elsayed MA, Gobara M (2016) Enhancement removal of tartrazine dye using? HCl-doped polyaniline and TiO_2-decorated PANI particles. Mater Res Express 3:085301

Fanchiang JM, Tseng DH (2009) Degradation of anthraquinone dye CI Reactive Blue 19 in aqueous solution by ozonation. Chemosphere 77:214–221

Gogate PR, Pandit AB (2004) A reviews of imperative technologies for wastewater treatment I: oxidation technologies at ambient conditions. Adv Environ Res 8:501–551

Golob V, Vinder A, Simonič M (2005) Efficiency of the coagulation/flocculation method for the treatment of dye bath effluents. Dyes Pigments 67:93–97

Guimarães JR, Maniero MG, de Araujo RN (2012) A comparative study on the degradation of RB-19 dye in an aqueous medium by advanced oxidation processes. J Environ 110:33–39

Guo Y, He D, Xia S, Xie X, Gao X, Zhang Q (2012) Preparation of a novel nanocomposite of polyaniline core decorated with anatase-TiO_2 nanoparticles in ionic liquid/water microemulsion. J Nanomater 2012:1–8

Hadjltaief HB, Galvez ME, Zina MB, Da Costa P (2014) TiO_2/clay as a heterogeneous catalyst in photocatalytic/photochemical oxidation of anionic Reactive Blue 19. Arab J Chem. https://doi.org/10.1016/j.arabjc.2014.11.006

Hidalgo D, Bocchini S, Fontana M, Saracco G, Hernández S (2015) Green and low-cost synthesis of PANI–TiO_2 nanocomposite mesoporous films for photoelectrochemical water splitting. RSC Adv 5:49429–49438

Huyen DN, Tung NT, Thien ND, Thanh LH (2011) Effect of TiO_2 on the gas sensing features of TiO_2/PANi nanocomposites. Sensors 11:1924–1931

Kabra K, Chaudhary R, Sawhney RL (2004) Treatment of hazardous organic and inorganic compounds through aqueous-phase photocatalysis: a review. Ind Eng Chem Res 43:7683–7696

Kamble SP, Sawant SB, Pangarkar VG (2003) Batch and continuous photocatalytic degradation of benzenesulfonic acid using concentrated solar radiation. Ind Eng Chem Res 42:6705–6713

Khan MAN, Siddiqu M, Wahid F, Khan R (2015) Removal of reactive blue 19 dye by sono, photo and sonophotocatalytic oxidation using visible light. Ultrason Sonochem 26:370–377

Khanna A, Shetty VK (2014) Solar light induced photocatalytic degradation of Reactive Blue 220 (RB-220) dye with highly efficient Ag@TiO_2 core–shell nanoparticles: a comparison with UV photocatalysis. Sol Energy 99:67–76

Khanna A, Shetty KV (2015) Solar light-driven photocatalytic degradation of anthraquinone dye-contaminated water by engineered Ag@TiO_2 core–shell nanoparticles. Desalin Water Treat 54:744–757

Kohut-Svelko N, Reynaud S, François J (2005) Synthesis and characterization of polyaniline prepared in the presence of nonionic surfactants in an aqueous dispersion. Synth Met 150:107–114

Kumar R, Ansari MO, Parveen N, Oves M, Barakat MA, Alshahri A, Cho MH (2016) Facile route to a conducting ternary polyaniline@TiO_2/GN nanocomposite for environmentally benign applications: photocatalytic degradation of pollutants and biological activity. RSC Adv 6:111308–111317

Li J, Zhu L, Wu Y, Harima Y, Zhang A, Tang H (2006) Hybrid composites of conductive polyaniline and nanocrystalline titanium oxide prepared via self-assembling and graft polymerization. Polymer 47:7361–7367

Li X, Wang D, Cheng G, Luo Q, An J, Wang Y (2008) Preparation of polyaniline-modified TiO_2 nanoparticles and their photocatalytic activity under visible light illumination. Appl Cata B 81:267–273

Lizama C, Freer J, Baeza J, Mansilla HD (2002) Optimized photodegradation of Reactive Blue 19 on TiO_2 and ZnO suspensions. Catal Today 76:235–246

Matthews RW (1991) Photooxidative degradation of coloured organics in water using supported catalysts. TiO_2 on sand. Water Res 25:1169–1176

Medien HA, Khalil SM (2010) Kinetics of the oxidative decolorization of some organic dyes utilizing Fenton-like reaction in water. J King Saud Univ Sci 22:147–153

Mohammadi M, Sabbaghi S (2014) Photo-catalytic degradation of 2, 4-DCP wastewater using MWCNT/TiO_2 nano-composite activated by UV and solar light. Environ Nanotechnol Monit Manag 1:24–29

Mozia S, Morawski AW, Toyoda M, Tsumura T (2009) Effect of process parameters on photodegradation of Acid Yellow 36 in a hybrid photocatalysis–membrane distillation system. Chem Eng J 150:152–159

Nabid MR, Golbabaee M, Moghaddam AB, Dinarvand R, Sedghi R (2008) Polyaniline/TiO_2 nanocomposite: enzymatic synthesis and electrochemical properties. Int J Electrochem Sci 3:1117–1126

Ozbay B, Genc N¸ Ozbay I, Baghaki B, Zor S (2016), Photocatalytic activities of polyaniline-modified TiO2 and ZnO under visible light: an experimental and modeling study. Clean Technol Environ, 18: 2591–2601

Pawar SG, Patil SL, Chougule MA, Mane AT, Jundale DM, Patil VB (2010) Synthesis and characterization of polyaniline: TiO_2 nanocomposites. Int J Polym Mater Polym Biomater 59:777–785

Priya S, Shanmuga AD, Dwarakanath R (2015) Visible light solar photocatalytic degradation of pulp and paper wastewater using dye-sensitised TiO_2. Int J Res Eng Technol 4:2321–7308

Radhakrishnan S, Siju CR, Mahanta D, Patil S, Madras G (2009) Conducting polyaniline–nano-TiO_2 composites for smart corrosion resistant coatings. Electrochim Acta 54:1249–1254

Radoičic M, Šaponjić Z, Janković IA, Ćirić-Marjanović G, Ahrenkiel SP, Čomor MI (2013) Improvements to the photocatalytic efficiency of polyaniline modified TiO_2 nanoparticles. Appl Catal B 136:133–139

Radoičić M, Šaponjić Z, Ćirić-Marjanović G, Konstantinović Z, Mitrić M, Nedeljković J (2012) Ferromagnetic polyaniline/TiO_2 nanocomposites. Polym Compos 33:1482–1493

Reddy KR, Nakata K, Ochiai T, Murakami T, Tryk DA, Fujishima A (2010) Nanofibrous TiO_2-core/conjugated polymer-sheath composites: synthesis, structural properties and photocatalytic activity. J Nanosci Nanotechnol 10:7951–7957

Reutergådh LB, Iangphasuk M (1997) Photocatalytic decolourization of reactive azo dye: a comparison between TiO_2 and us photocatalysis. Chemosphere 35:585–596

Rezaee A, Taghi Ghaneian M, Jamalodin Hashemian S, Moussavi G, Khavanin A, Ghanizadeh G (2008) Decolorization of reactive blue 19 dye from textile wastewater by the UV/H2O2 process. J App Sci 8:1108–1112

Rezaee A, Ghaneian MT, Taghavinia N, Aminian MK, Hashemian SJ (2009) TiO_2 nanofibre assisted photocatalytic degradation of Reactive Blue 19 dye from aqueous solution. Environ Technol 30: 233–239

Robinson T, McMullan G, Marchant R, Nigam P (2001) Remediation of dyes in textile effluent: a critical review on current treatment technologies with a proposed alternative. Bioresour Technol 77: 247–255

Salem MA, Al-Ghonemiy AF, Zaki AB (2009) Photocatalytic degradation of allura red and quinoline yellow with polyaniline/TiO_2 nanocomposite. Appl Catal B 91:59–66

Sandhya KP, Haridas S, Sugunan S (2014) Visible light induced photocatalytic activity of polyaniline modified TiO_2 and Clay-TiO_2 composites. Bull Chem React Eng Catal 8:145–153

Sarmah S, Kumar A (2011) Photocatalytic activity of polyaniline-TiO_2 nanocomposites. Indian J Phys 85:713–726

Sauer T, Neto GC, Jose HJ, Moreira RFPM (2002) Kinetics of photocatalytic degradation of reactive dyes in a TiO_2 slurry reactor. J Photochem Photobiol 149:147–154

Senadeera GKR, Kitamura T, Wada Y, Yanagida S (2004) Deposition of polyaniline via molecular self-assembly on TiO_2 and its uses as a sensitiser in solid-state solar cells. J Photochem Photobiol 164:61–66

Shet A, Shetty KV (2016) Photocatalytic degradation of phenol using Ag core-TiO_2 shell (Ag@TiO_2) nanoparticles under UV light irradiation. Environ Sci Pollut Res. 23:20055–20064

Stejskal J, Kratochvil P, Radhakrishnan N (1993) Polyaniline dispersions 2. UV-Vis absorption spectra. Synth Met 61:225–231

Trchová M, Stejskal J (2011) Polyaniline: the infrared spectroscopy of conducting polymer nanotubes (IUPAC Technical Report). Pure Appl Chem 83:1803–1817

Trchová M, Šeděnková I, Konyushenko EN, Stejskal J, Holler P, Ćirić-Marjanović G (2006) Evolution of polyaniline nanotubes: the oxidation of aniline in water. J Phys Chem B 110:9461–9468

Vidhyakalarani R, Premaraj S (2013) Microbial decolorization of azo dye reactive blue 19. Int J Curr Microbiol App Sci 2:370–372

Wang D, Zhang J, Luo Q, Li X, Duan Y, An J (2009) Characterization and photocatalytic activity of poly (3-hexylthiophene)-modified TiO_2 for degradation of methyl orange under visible light. J Hazard Mater 169:546–550

Xia Y, Wiesinger JM, MacDiarmid AG, Epstein AJ (1995) Camphorsulfonic acid fully doped polyaniline emeraldine salt: conformations in different solvents studied by an ultraviolet/visible/near-infrared spectroscopic method. Chem Mater 7:443–445

Yasmina M, Mourad K, Mohammed SH, Khaoula C (2014) Treatment heterogeneous photocatalysis; factors influencing the photocatalytic degradation by TiO_2. Energy Procedia 50:559–566

Yu QZ, Wang M, Chen HZ, Dai ZW (2011) Polyaniline nanowires on TiO_2 nano/microfiber hierarchical nano/microstructures: preparation and their photocatalytic properties. Mater Chem Phys 129:666–672

Yue J, Wang ZH, Cromack KR, Epstein AJ, MacDiarmid AG (1991) Effect of sulfonic acid group on polyaniline backbone. J Am Chem Soc 113:2665–2671

Zhang L, Liu P, Su Z (2006) Preparation of PANI–TiO_2 nanocomposites and their solid-phase photocatalytic degradation. Polym Degrad Stab 91:2213–2219

Zhang H, Zong R, Zhao J, Zhu Y (2008) Dramatic visible photocatalytic degradation performances due to synergetic effect of TiO2 with PANI. Environ Sci Technol 42:3803–3807